Engineering Letters

Enhanced Humidity Sensing Utilizing Tin Oxide Nanoparticles Embedded in a Seaweed Polymer Matrix

I Dewa Putu Hermida, Goib Wiranto, Desak Gede Sri Andayani, Deviana Agustina, Rizki Deva Berlian, Irzaman, Asrul Izam Azmi, Sevia Mahdaliza Idrus Sutan Nameh, *Member, IAENG*

***Abstract*—Humidity monitoring is essential due to the significant variations in environmental conditions, making the development of high-performance sensors a priority. Therefore, this study was aimed to enhance humidity sensing capabilities using tin dioxide (SnO_2) nanoparticles embedded in a seaweed-derived sodium alginate polymer matrix. SnO_2, known for its high reactivity to water molecules, was synthesized using hydrothermal method, yielding nanoparticles with an average size of 8.9 nm. A natural polymer matrix has been used because of its hydrophilic properties and biodegradability, besides cost-effectiveness, to enhance the sensor's responsiveness and sensitivity. The sensors were fabricated using thick film technology with Silver-Palladium (AgPd) electrodes, selected for their superior conductivity, stability, and low ion migration. The structural and morphological properties of the SnO_2 nanoparticles were characterized using X-Ray Diffraction (XRD) and Scanning Electron Microscopy (SEM). The results showed that XRD analysis confirmed the tetragonal structure with sharp diffraction peaks, indicating high crystalline structures. Meanwhile, SEM result showed a rough and porous surface, beneficial for water molecule interaction. The AgPd electrodes demonstrated excellent adhesion and a uniform coating with a thickness of 7.097 µm, contributing to improved conductivity and durability. Sensors performance was then evaluated under a controlled Styrofoam chamber using Keithley 6517B electrometer. The results showed high sensitivity and rapid responses, with a response time of 208 seconds and a recovery time of 162 seconds for relative humidity (RH) ranging from 60% to 90%. Sensitivity analysis showed that thinner sensing layers, specifically at 10 mg doping mass, had higher responsiveness due to greater surface area-to-volume ratio. However, for 20 mg doping mass, it showed the highest resistance at low humidity, indicating optimal sensitivity for applications requiring precise humidity detection. This study has shown the efficacy of SnO_2 nanoparticles and seaweed-based polymers in enhancing the sensor's performance. The results indicated that doping mass significantly influenced sensors behavior, with thinner layers providing rapid responses and thicker layers offering enhanced sensitivity. The integration of natural polymers with metal oxide nanoparticles thus presented a promising method for developing sustainable, high-performance humidity sensors suitable for diverse environmental applications. The low production cost further enhanced the potential for widespread application in environmental monitoring, industrial control, and healthcare.**

***Index Terms*—humidity sensors, low-cost production, seaweed, SEM, SnO_2 nanoparticles**

I. INTRODUCTION

Humidity can be defined as the concentration of water vapor present in the atmosphere, and its measurement is usually termed hygrometry [1]. Humidity monitoring is essential due to a significant variation across different environments. Thus, an accurate measurement of humidity is important to ensure optimal conditions and safety in various fields, including agriculture, transportation, healthcare, and infrastructure [2].

Historically, humidity sensors have been used since 1983 and since then have evolved considerably in terms of technology and application [3]. The sensor measurement is commonly expressed as a percentage of relative humidity (RH%), which represents the ratio of the current amount of water vapor in the air to the maximum amount that the air can hold at a given temperature [4]. Generally, an ideal humidity sensor should be highly sensitive, robust, and physically and chemically stable. It must also be rapid in response time, and quick in recovery time, which serves as essential tools in environments where precise humidity control is required [5].

The performance of humidity sensors is influenced by several factors, including the morphological structure of the surface, the material used as the sensing layer, and the manufacturing process [6]. These factors thus determine the sensors effectiveness for various applications, particularly in human health monitoring, where sensors are increasingly used to detect respiratory conditions and monitor skin moisture levels. Humidity requirements also vary based on

Manuscript received September 30, 2024; revised Apr 09, 2025. This work was supported in part by the National Research and Innovation Agency (BRIN), Republic of Indonesia.

I Dewa Putu Hermida is a PhD student at the Faculty of Electrical Engineering, Universiti Teknologi Malaysia, 81310, Johor Bahru, Malaysia (email: iputu@graduate.utm.my).

Goib Wiranto is a research professor at the Research Center for Electronic, National Research and Innovation Agency, Kawasan Sains dan Teknologi Samaun Samadikun, Bandung-40135, Indonesia (email: gwiranto@gmail.com).

Desak Gede Sri Andayani is a senior researcher (Ph.D) specializing in natural polymer synthesis at the Research Center for Environmental and Clean Technology, National Research and Innovation Agency, BJ Habibie Science and Technology Area, Building 820, Serpong, South Tangerang-15314, Indonesia (email: desa001@brin.go.id).

Deviana Agustina is an undergraduate at the Department of Physics, IPB University, Kampus Dramaga, Bogor-16680, Indonesia (email: devianaagustina@apps.ipb.ac.id).

Rizki Deva Berlian is an undergraduate at the Department of Physics, IPB University, Kampus Dramaga, Bogor-16680, Indonesia (email: rizkidevaberlian@apps.ipb.ac.id).

Irzaman is a professor of Applied Physics at the Department of Physics, IPB University, Kampus Dramaga, Bogor-16680, Indonesia (email: irzaman@apps.ipb.ac.id).

Asrul Izam Azmi is an associate professor of Optical Sensor at the Faculty of Electrical Engineering, Universiti Teknologi Malaysia, 81310, Johor Bahru, Malaysia (email: asrul@utm.my).

Sevia Mahdaliza Idrus Sutan Nameh is a professor of Optical Communication Systems and Optoelectronics at the Faculty of Electrical Engineering, Universiti Teknologi Malaysia, 81310, Johor Bahru, Malaysia (email: sevia@utm.my).

the environment. For example, RH level below 45% indicates a dry environment that promotes water evaporation, while levels above 80% can inhibit this process, leading to discomfort or potential health issues.

Many kinds of materials have been used for resistive-type humidity sensors, including metal oxides, conductive polymers, ceramics, carbon-based, and nanomaterials [7]. Among these materials, tin dioxide (SnO_2) is superior due to high reactivity to water molecules, thermal stability, and has diverse chemical properties. SnO_2 is an n-type semiconductor with a relatively large bandgap of approximately 3.6 eV in its rutile tetragonal structure. Therefore, SnO_2 is suitable for a wide range of applications, including humidity sensors, gas and light detectors, biosensors, catalysts, and lithium-ion batteries [8]. Different forms of SnO_2 materials have been used to develop humidity and gas sensors. For example, a resistive humidity sensor was developed using SnO_2 nanostructured thin film fabricated by spin-coating method, which achieves a high sensitivity of 1.34 kΩ/%RH, minimal hysteresis of 0.94%, and a stable performance with response and recovery times of 84 seconds and 576 seconds, respectively, making it suitable for real-time respiratory monitoring [8]. In other reports, resistive gas sensors using carbon-modified SnO_2 nanowires grown by CVD (chemical vapor deposition) showed high accuracy in gas classification and effective concentration estimation, assisted by machine-learning methods [9].

Various metal-doped SnO_2 nanostructures have been proposed to enhance humidity sensing performance. These include a study on the synthesis of copper-doped SnO_2 through chemical precipitation, showing that annealing at 600°C achieved the highest sensitivity due to enhanced crystallite size and surface area [10]. Another report showed that reduced graphene oxide decorated with Fe-doped SnO_2 nanoparticles, synthesized through electrostatic interaction, significantly enhanced the sensitivity and performance of resistive humidity sensors compared to undoped SnO_2 due to the synergistic effects of the composite structure [6]. Furthermore, zinc-doped tin oxide (Zn-SnO_2) nanoparticles have been synthesized using chemical coprecipitation. The results showed high humidity monitoring performance due to enhanced porosity and oxygen vacancies created by calcination at 500°C [11]. These studies show that doping SnO_2 with various metals significantly enhances humidity monitoring capabilities by improving the structural, electronic, and surface properties of the sensing materials.

The use of nanocomposite materials, which combine polymers with nanoparticles or metal oxides to enhance sensor performance, also constantly received strong interest. A resistive humidity sensor using thin film of carbon-black and polyvinyl alcohol composite was developed by Zhang et al. to achieve a rapid response time of approximately 5.77 seconds and high sensitivity across a humidity range of 10.9% to 73.7% RH [12]. In another report, a humidity sensor using crystalline tin oxide nanoparticles encapsulated in a polyaniline matrix was synthesized by Shukla et al., achieving an enhanced sensitivity of $0.22\%RH^{-1}$, a response time of 26 seconds, and a recovery time of 30 seconds [13]. A composite of chitosan, graphene oxide, and SnO_2 has also been used to fabricate a high-sensitivity humidity sensor with a fast response time [14]. Additionally, resistive humidity sensors based on a hybrid nanocomposite of PVDF and ZnO nanoparticles [15], as well as nickel-containing metal-polymer nanocomposites [16], were able to improve sensor performance.

The trend of using natural polymers in manufacturing industries, particularly for humidity sensor applications, has increased recently due to their various benefits. These include biodegradability, biocompatibility, abundant availability, cost-effectiveness, and high sensitivity to moisture. Natural polymers have the potential to be used as independent humidity sensing or combined with various nanomaterials to enhance sensors performance. Humidity sensors using gelatin and carbon black nanoparticles were also designed to achieve rapid response and recovery times of less than 10 seconds, with high sensitivity across a relative humidity range of 20.3% to 83.2% [17]. Other related studies have developed flexible resistive humidity sensors using natural polymers, such as carbonized lignin combined with sodium alginate, achieving ultra-high sensitivity and stable repeatability in a wide RH range of 11 to 97% [18]. Similarly, chitosan-based sensors printed on flexible thermoplastic polyurethane substrates have shown high sensitivity and stability, with a broad humidity detection range of 20% to 90% RH [19].

Based on the above description, this study was aimed to develop high-performance humidity sensors using SnO_2 nanoparticles and natural polymers derived from seaweed, specifically sodium alginate, as the sensing material. The SnO_2 nanoparticles were synthesized using hydrothermal method, leading to highly crystalline particles, which provided a large surface area to enhance the interaction with water molecules. Seaweed-based polymers have been selected for their excellent hydrophilic properties, significantly enhancing the sensitivity and response of sensors to humidity changes. These sensors were then fabricated using thick film technology with silver-palladium (AgPd) electrodes, showing excellent performance, including high sensitivity, rapid response, and stability over a wide humidity range.

II. MATERIALS

SnO_2 material features a tetragonal structure with hexagonal coordination for Sn ions and triple coordination for O atoms. It has a molar mass of 150.71 g/mol, a melting point of approximately 1630°C, a boiling point of 1900°C, and a density of 6.95 g/cm³. The high electron mobility of SnO_2 facilitates rapid electron transfer reactions, which are essential for efficient sensing operations [20].

The physical and chemical stability of SnO_2 exceeds other materials. The intrinsic n-type conductivity, attributed to the presence of oxygen vacancies and Sn interstitials, plays an essential role in the adsorption and desorption of water molecules, which is fundamental to the sensing mechanism [21]. Fig. 1 shows the structural and functional characteristics of SnO_2 in humidity-sensing applications.

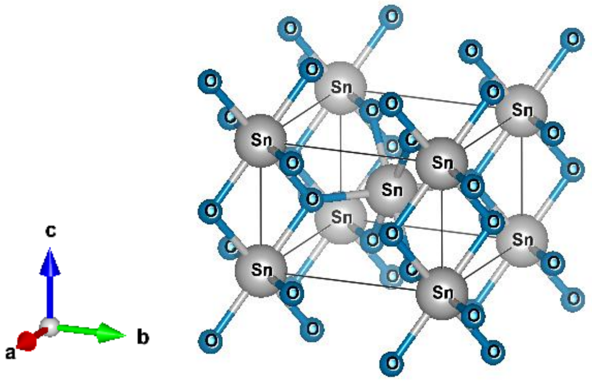

Fig. 1. SnO_2 rutile structure

Fig. 2 shows the interaction mechanism between a seaweed-doped SnO_2 thin layer and water molecules (H_2O), which is essential for effective humidity monitoring. In the initial stages, the water molecules form robust chemical bonds with the surface of the SnO_2 material, leading to the formation of a chemisorbed layer. Subsequently, additional water molecules attach through comparatively weaker hydrogen bonds, forming the initially physisorbed and a secondary layer. As humidity levels rise, these layers expand. The adsorption of water molecules alters the electrical properties of the SnO_2 layer, enabling humidity sensors to detect changes in the surrounding environment. The doping of SnO_2 with seaweed enhances sensitivity and selectivity by increasing the active sites for water adsorption and promoting hydrogen bond formation, thereby improving humidity detection.

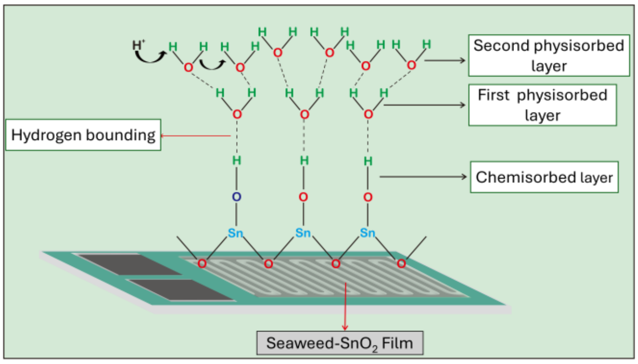

Fig. 2. Humidity-sensing mechanism that occurs because of the interaction between water molecules and SnO_2

III. EXPERIMENT

In this study, SnO_2 nanoparticles and natural polymers derived from seaweed were used as the sensing layer. The experimental process was divided into 2 stages, namely material synthesis and sensors fabrication. In the material synthesis stage, SnO_2 nanoparticles were synthesized using the hydrothermal method. Additionally, natural seaweed-based materials were synthesized and used as sensing materials. Finally, humidity sensors were fabricated using thick film technology.

A. Fabrication of AgPd Electrode Sensor

Silver-palladium (AgPd) paste is a material that is widely used in the context of thick film technology due to its superior properties compared to pure silver paste. Additionally, AgPd paste is the preferred material for connecting electrode lines and pads in sensors as well as electronic devices due to low electron migration characteristics. This ensures that the particles remain stable during long-term use, thereby allowing electrical and mechanical stability [22].

The excellent adhesion of AgPd to substrates such as alumina enhances device durability and reliability. Despite the higher sheet resistance in comparison to pure silver, the strong adhesion and lower ion migration make AgPd an optimal option for thick film applications [8, 23]. When applied through screen printing and subjected to heat treatment, the paste forms solid conductive paths, which reduces sensor resistance and improves performance [23].

B. Synthesis SnO_2 Nanoparticles

The synthesis of SnO_2 nanoparticles was conducted using the hydrothermal method, which enabled the production of nanoparticles with high crystallinity and purity. The materials used in the synthesis consisted of $SnCl_4.5H_2O$, NaOH, and deionized water as precursor, reagent, and solvent, respectively. A total of 0.26 M $SnCl_4.5H_2O$ and 1.3 M NaOH were separately prepared by dissolving each in 50 ml of deionized water. The $SnCl_4.5H_2O$ solution was agitated using a magnetic stirrer for 45 minutes, followed by the gradual addition of NaOH solution. Initially, the solution was transparent and further changed color to white after adding NaOH. Once the stirring process was complete, the solution was transferred into a Teflon-lined stainless-steel autoclave with a capacity of 100 ml. The autoclave was placed in an oven set to 160°C for 12 hours, after which it was cooled to room temperature. Subsequently, the solution passed through a filtration process, whereby the gel-like precipitate was washed with ethanol and deionized water to remove contaminants and unwanted compounds. The precipitate obtained was subjected to a drying process at 100°C for 6 hours to remove the solvent, followed by a calcining process at 500°C for 3 hours to enhance its crystal structure. The calcined material was pulverized using an agate mortar for 5 hours. Fig. 3 shows the details regarding the hydrothermal process.

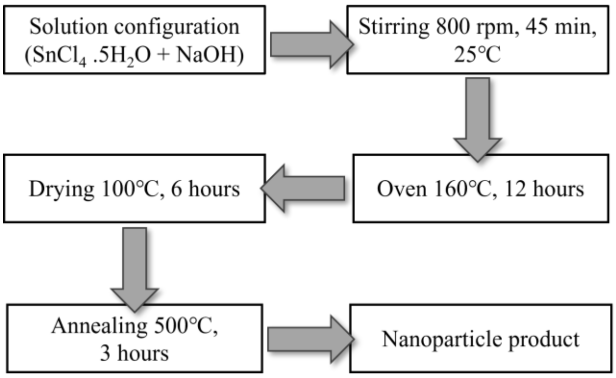

Fig. 3. Flow chart of a hydrothermal method

C. Seaweed

The synthesis of seaweed extracts shows suitability as moisture sensor polymer materials due to distinctive properties that facilitate efficient moisture detection capabilities. Firstly, these extracts contain polysaccharides, including alginate, which act as hydrogels or superabsorbent polymers (SAP). Hydrogels comprise a 3-dimensional network capable of absorbing and retaining substantial quantities of water, which is 200 times their weight while maintaining insolubility and pressure resistance. This enables seaweed-based sensors to respond rapidly and accurately to humidity fluctuations, as the material efficiently absorbs and releases water molecules. Secondly, the presence of hydrophobic and hydrophilic functional groups in the seaweed polymer structure, such as carboxyl (-COOH) and hydroxyl (-OH) groups, enables strong interactions with water molecules, causing measurable changes in electrical properties (capacitance or resistance) [24-27].

The biocompatibility, biodegradability, and non-toxic nature of seaweed extracts are environmentally friendly alternatives to synthetic polymer materials. Additionally, doping with other conductive materials, such as SnO_2, can enhance sensitivity and selectivity to moisture. The use of seaweed-based polymer thin films or coatings has demonstrated favorable performance in various moisture sensor applications, including in environmental and health monitoring [28].

IV. RESULT AND DISCUSSION

A. Characterization of SnO_2

The synthesis of SnO_2 nanoparticles was completed using the hydrothermal method with $SnCl_4.5H_2O$ as the precursor. The chemical reaction involved in the formation of SnO_2 is represented as follows:

$$SnCl_4 + 4NaOH \rightarrow Sn(OH)_4 \downarrow + 4NaCl \qquad (1)$$

$$Sn(OH)_4 \rightarrow SnO_2 + 2H_2O \qquad (2)$$

When $SnCl_4$ reacts with NaOH, a balance is achieved between the excess hydroxide ions (OH^-) from NaOH and hydrogen ions (H^+) from $SnCl_4$, causing a neutralization reaction. In this process, $SnCl_4$ reacts with NaOH, which is a strong base. Ion exchange occurs between the 2 compounds, forming tin (IV) hydroxide ($Sn(OH_4)$) as the main product and sodium chloride (NaCl) as a by-product, as shown in equation (1). The $Sn(OH)_4$ passes through decomposition, due to heat or specific environmental conditions. When exposed to heat, the $Sn(OH)_4$ molecule will experience a loss of some or all of its hydroxide ions, leading to the formation of the main product, tin (IV) oxide (SnO_2), and water (H_2O) as a by-product, as shown in equation (2). This is a chemical change that occurs when the $Sn(OH)_4$ molecule is divided into SnO_2 and water, which represent solid and liquid compounds, respectively. The process shows the effectiveness of the hydrothermal method in producing pure-phase SnO_2 nanoparticles, as the main by-product is NaCl, which is readily soluble in water and lost after the synthesis process.

In this study, the Malvern Zetasizer Nano-ZS was used to analyze SnO_2 nanoparticles, obtaining an average particle size distribution of 8.9 nm. The small particle size and large specific surface area of these materials facilitate interactions with water molecules, showing potential for use in moisture sensors. The use of water with a refractive index of 1.33 and SnO_2 of 1.993 during the characterization process prevented agglomeration. Furthermore, the hydrothermal method showed efficacy in the synthesis of SnO_2 nanoparticles with particle sizes below 100 nm [29], see Fig. 4.

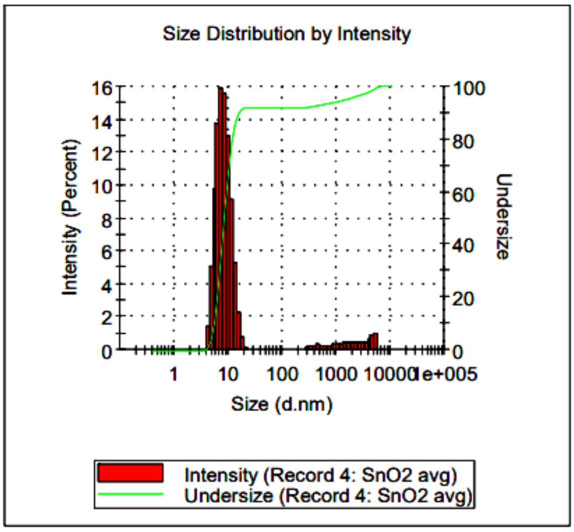

Fig. 4. Particle size distribution of SnO_2

The SnO_2 nanoparticles, which have been successfully synthesized, are subjected to characterization using X-Ray Diffraction (XRD) on a Bruker D8 Advance 3kW with a LynxEye XE-T detector and a Cu Kα radiation source. XRD is a method that uses X-rays to differentiate crystal atoms within a sample, forming diffraction patterns at distinct angles. These patterns can help elucidate the intrinsic characteristics of the tested samples. The XRD characterization results were analyzed to determine the inter-atomic distance, full width at half maximum (FWHM), and dominant peaks in each sample.

The XRD pattern of SnO_2 nanoparticles is shown in Fig. 5. Based on the results, sharp diffraction peaks were observed at angles of 26.55°, 33.90°, 37.98°, 51.84°, and 54.72° could be attributed to the (110), (101), (200), (211), and (220) planes, respectively. These observations correlated with the ICDD PDF4+ data. All peaks were identified as tetragonal structures for the sample calcined at 500°C with an average SnO_2 nanoparticles crystal size of 17 nm. The crystal lattice parameters were calculated by the method Cramer-Cohen leading to the following values: a = 4.73249 Å and c = 3.17605 Å. Broad peaks were observed in the XRD pattern due to the small crystallite size, along with sharp peaks indicative of good crystalline properties. However, no impurities were identified in the SnO_2 nanoparticles.

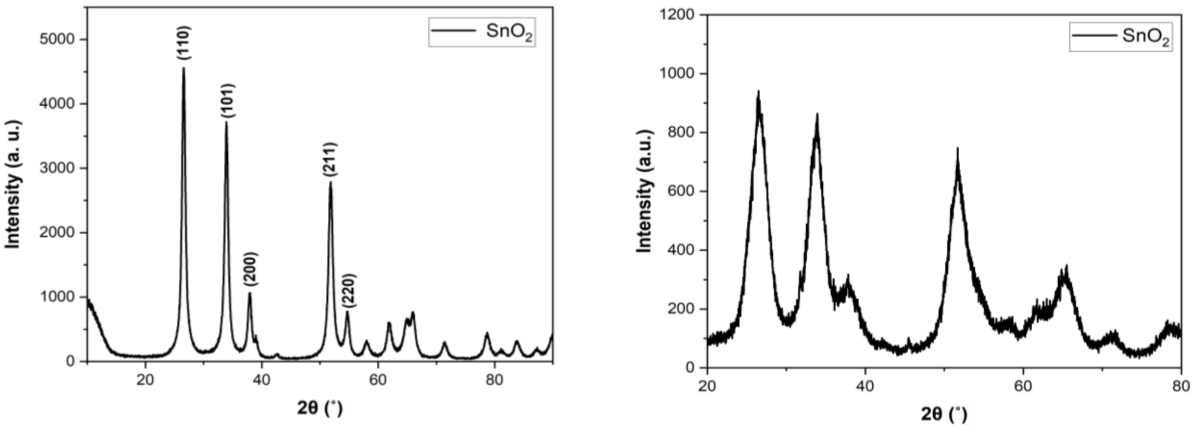

(a)

(b)

Fig. 5. XRD diffractogram of SnO_2 nanoparticles (a) after (b) before calcination

TABLE I
COMPARISON OF XRD PARAMETERS OF SYNTHESIZED SnO_2 WITH INTERNATIONAL CENTRE FOR DIFFRACTION DATA (ICDD)

2θ	hkl	SnO_2 synthesis result	ICDD
		d-spacing (Å)	d-spacing (Å)
26.55	110	3.3457	3.3504
33.90	101	2.6375	2.6445
37.98	200	2.3685	2.3691
51.84	211	1.7622	1.7645
54.72	220	1.6768	1.6752

Table I shows a comparison between the diffraction angle (2θ) and d-spacing values obtained from the synthesized SnO_2 with standard reference values sourced from the International Center for Diffraction Data (ICDD). The 2θ value shown for each diffraction peak (*hkl*) in the synthesized SnO_2 sample is identical to the values in the ICDD database. This suggests that the crystal phase formed in the sample is SnO_2 with a structure matching the reference. Furthermore, the d-spacing values of the synthesized SnO_2 samples are extremely close to the values listed in the ICDD. The results showed that the synthesis process successfully produced SnO_2 crystals with a structure like internationally recognized standards.

TABLE II
THE RESULTS OF THE PHASE IDENTIFICATION OF SnO_2 NANOPARTICLES USING THE MATCH SOFTWARE

Compound	Tin (IV) Oxide
Crystal	Tetragonal
Unit cell	a = 4.73249 Å, c = 3.17605 Å
Intensity scale factor	0.69
2θ shift	0.030°

As shown in Table II, the MATCH software successfully identified the analyzed material as SnO_2 with a tetragonal crystal structure, consistent with the expected characteristics of this compound. The calculated unit cell parameters, specifically a and c, indicated that the dimensions of the SnO_2 crystal lattice closely correlated with known values for the tetragonal structure of SnO_2. This confirmed the successful synthesis of the desired material. The slightly lower intensity scale factor (0.69) may reflect either the crystal quality or a slightly lower-than-anticipated sample quantity, although it remains within the acceptable range for phase identification. In Fig. 6, minor shifts in the 2θ angle suggest the possible presence of imperfections or internal stresses in the crystal. However, these shifts are minimal and do not significantly affect phase identification.

Based on Fig. 6, Scanning Electron Microscopy (SEM) of SnO_2 nanoparticles shows a broad range of particle sizes, spanning from the nanometre to the micrometer scale. Although several particles show a spherical morphology, some have irregular shapes. The nanoparticles' surfaces appear rough and porous, a characteristic typical of materials synthesized through hydrothermal or wet chemical methods. This porosity enhances the specific surface area and is crucial for applications such as sensors and catalysts. However, the nanoparticles tend to agglomerate, forming larger clusters due to van der Waals forces or sample handling. The reaction can potentially reduce their effectiveness in applications requiring uniform particle dispersion. The observed structural uniformity indicates the successful completion of the synthesis process, but further optimization is required to achieve more precise control over particle size and shape. The SEM analysis confirms that the high surface area makes SnO_2 nanoparticles highly advantageous for incorporation in gas and humidity sensor applications, due to their enhanced sensitivity to environmental fluctuations [5, 6].

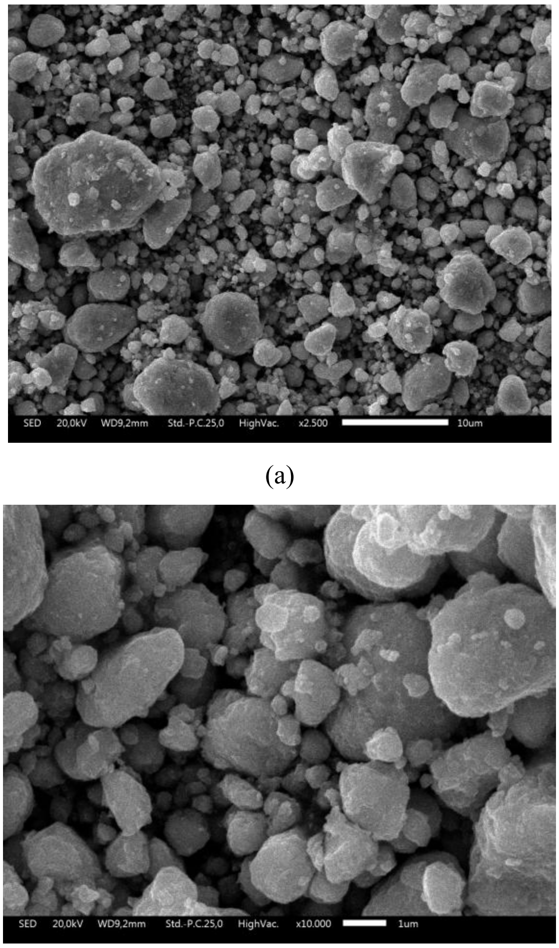

(a)

(b)

Fig. 6. Morphology of SnO_2 nanoparticles SEM magnification (a) 2500x, (b) 10.000x (*Scanning Electron Microscopy* (SEM) type JEOL JSM IT300LV)

A. *Characterization of Electrode AgPd*

AgPd paste is frequently used in thick film technology due to its improved qualities over pure silver. Due to low migration qualities, AgPd paste is recommended for joining electrode lines and pads in sensors as well as electronic devices, ensuring electrical and mechanical stability during long periods of operation [23]. It also has great adherence to surfaces such as alumina, which increases device longevity and dependability. Despite having higher sheet resistance than pure silver, the excellent adhesion and low ion migration make AgPd ideal for thick film applications [8, 23]. When applied through screen printing and heated, the paste generates solid conductive channels, lowering sensor resistance and boosting performance [23].

Fig. 7 shows that AgPd electrode's SEM results indicate the presence of a surface layer with a thickness of 7.097 µm. The layer is characterized by a high concentration of silver and palladium, showing a distinctive, rough, and variable microscopic structure. Furthermore, the layer is considered essential for applications that require conductivity and corrosion resistance, such as in high-precision electrical connectors. The consistency and quality of the coating have a profound impact on the long-term performance of the electrode. This SEM analysis provides invaluable insights into evaluating the quality of such materials.

AgPd electrodes are highly resistant to environmental degradation, such as oxidation and corrosion. Therefore, the electrodes are reliable for long-term use in various electronic and sensor applications. The use of thick film technology allows the manufacture of electrodes in more complex shapes and is cost-flexible, particularly in large-scale production. In humidity sensors, AgPd electrodes can ensure efficient signal transfer and rapid response to changes in environmental humidity.

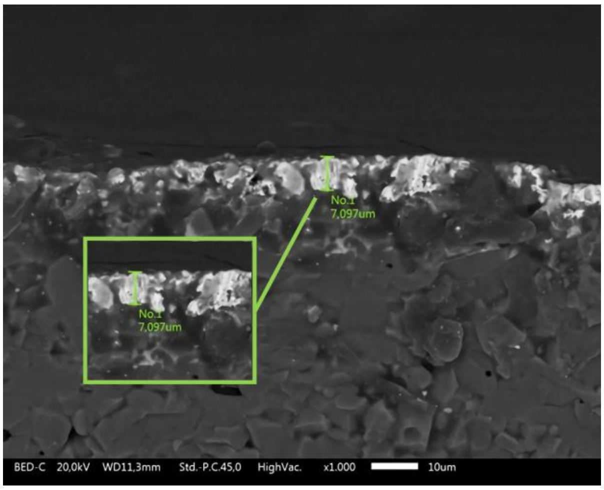

Fig. 7. Measurement of the thickness of the AgPd electrode using SEM at 1000x magnification. (*Scanning Electron Microscopy* (SEM) type JEOL JSM IT300LV)

Fig. 8. shows the result of SEM analysis with Energy Dispersive X-ray Spectroscopy (EDS/EDX) used for elemental mapping on the sample surface. The SEM image shows the texture and topography of the sample, where the elemental map uses different colors to indicate the distribution of elements. These include tin (Sn), carbon/seaweed (C), aluminum (Al), palladium (Pd), silver (Ag), and oxygen (O), which are indicated in yellow, red, blue, purple, magenta, and green, respectively. Fig. 9 shows a layered structure with palladium on top and an oxide layer below, indicating a possible metal coating or chemical reaction such as oxidation or alloy formation.

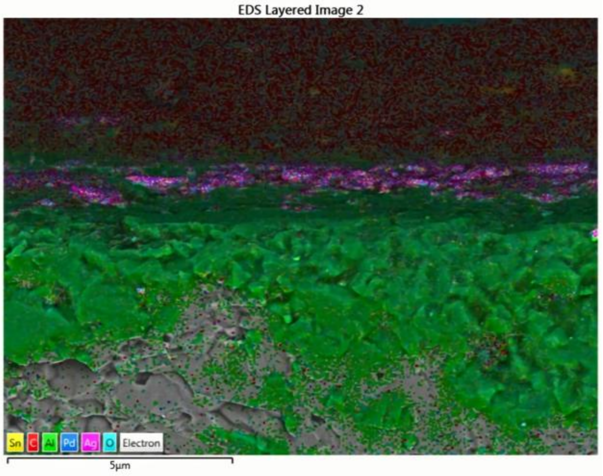

Fig. 8. Elemental distribution on the sample surface from SEM-EDS analysis (JEOL JSM IT300LV).

Fig. 9 shows EDS mapping results indicating the distribution of chemical elements in the sample. Each color represents a specific element distributed in the mapped area. Brief explanation:

- Red: Possible carbon (C), indicating seaweed sensing material.
- Cyan: Possible oxygen (O).

- Green: Possible aluminum (Al), indicating part of the Al_2O_3 substrate.
- Dark Blue: Possible palladium (Pd), indicating part of the AgPd finger.
- Purple: Possible silver (Ag), indicating part of the AgPd finger.
- Yellow: Possible tin (Sn), indicating part of the SnO_2 metal oxide material.

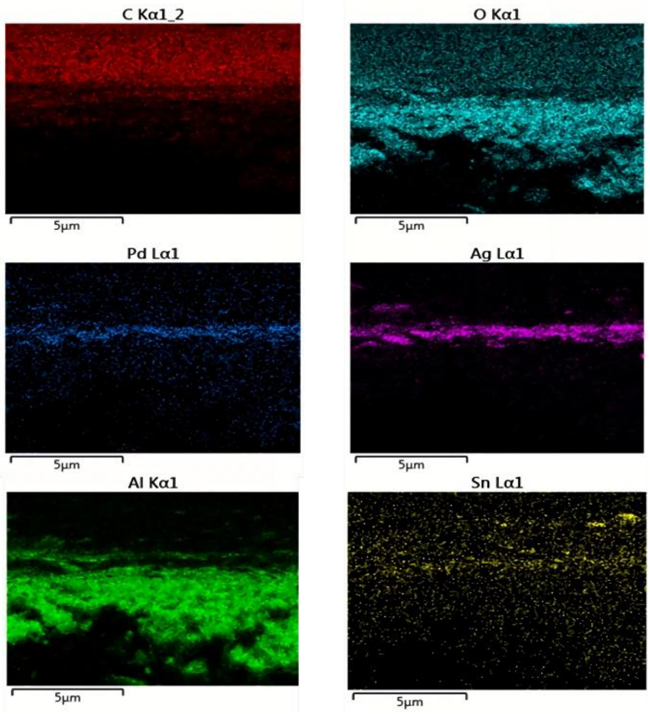

Fig. 9. EDS mapping results showing the distribution of chemical elements in the sample

Fig. 10 shows the method for evaluating humidity sensors functionality within a Styrofoam chamber, including several key steps. Initially, sensors to be tested are installed in an isolated chamber to maintain stable humidity and temperature, allowing for accurate assessment of its accuracy, sensitivity, stability, and response to RH. Reference sensors, including humidity sensors and a thermocouple, are also placed in the chamber. An air humidifier raises the humidity level, with fluctuations managed by a microcontroller through a power outlet. A Keithley 6517B device, connected to sensors through a GPIB interface, measures the sensors response as voltage or current. Subsequently, data are acquired and analyzed using Python software on a PC or laptop, producing graphs that depict the sensors response to humidity changes. This analysis helps determine key parameters like sensitivity, response time, and stability. At 5V, the current ranges from 20 µA (low resistance, 90% RH) to 20 mA (high resistance, 60% RH) [16].

As presented in Fig. 11, the XRD analysis of the SnO_2 nanoparticles showed that the sample was composed of 100% cassiterite (SnO_2) phase with an elemental composition of 78.8% Sn and 21.2% O by weight. The analysis was conducted within the 2θ angle range of 10.073° to 90.045°, including 3920 data points with a step size of 0.020°. In Fig. 13, the data were processed using the Rietveld refinement method, consolidated with an X-ray wavelength of 1.541874 Å. This phase purity demonstrates the absence of contamination from others, indicating that the crystal structure formed is uniform and follows the expected model.

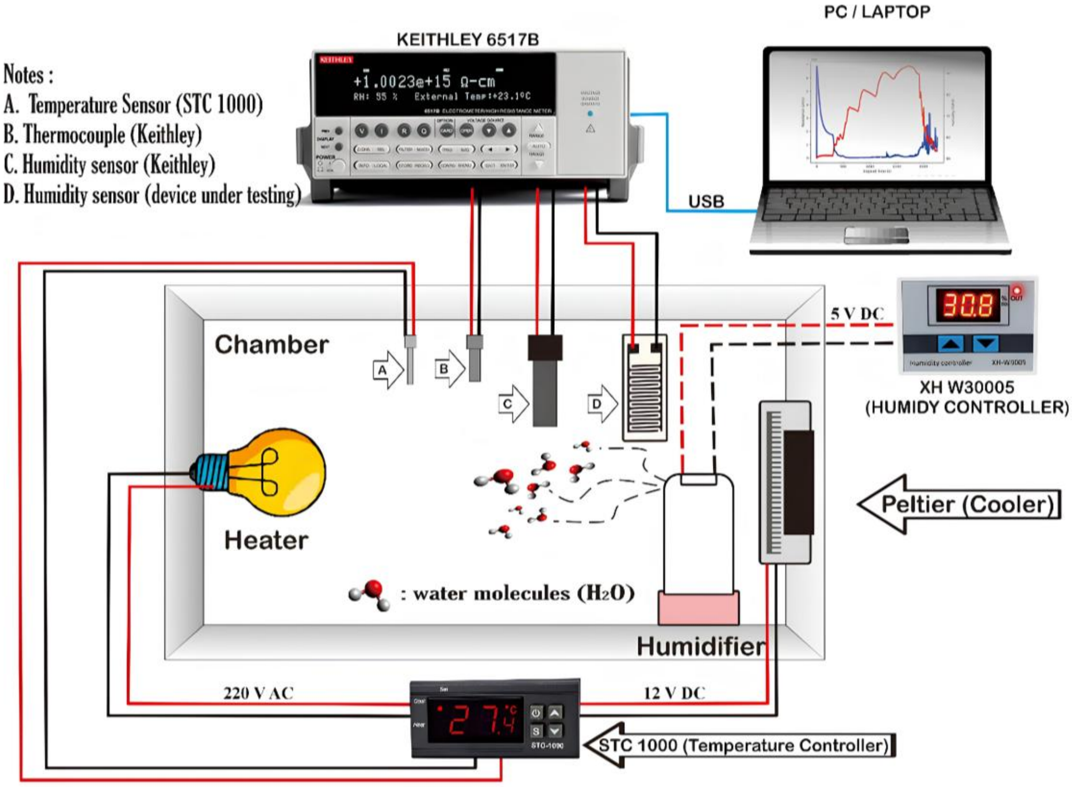

Fig. 10. Schematic of humidity sensor testing using a chamber

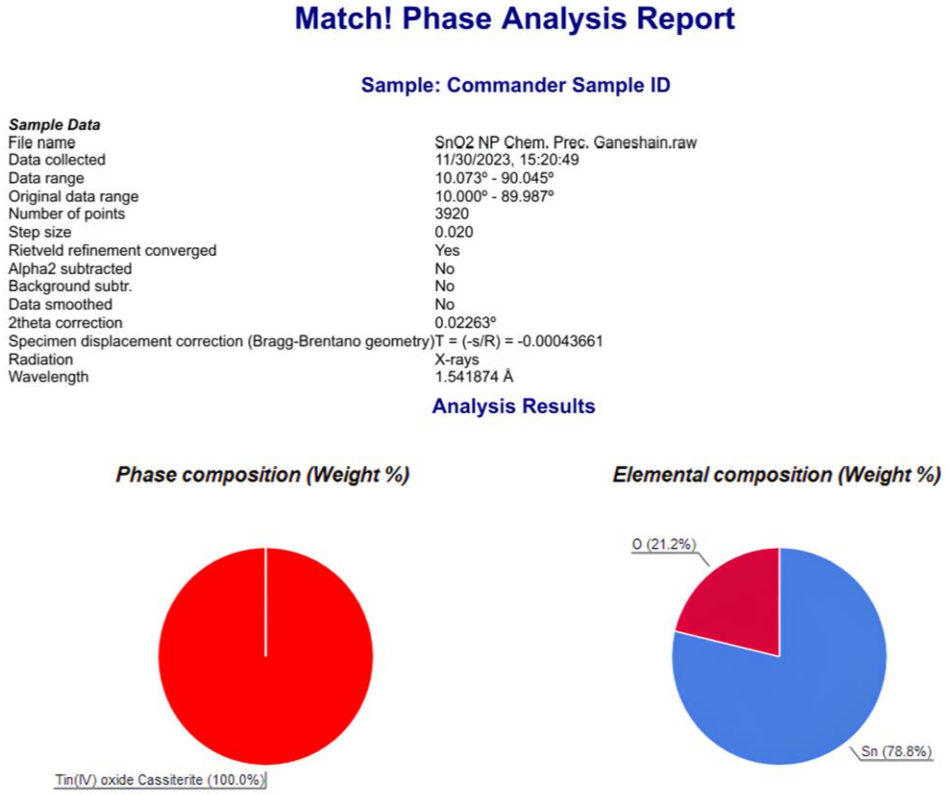

Match! Phase Analysis Report

Sample: Commander Sample ID

Sample Data	
File name	SnO2 NP Chem. Prec. Ganeshain.raw
Data collected	11/30/2023, 15:20:49
Data range	10.073° - 90.045°
Original data range	10.000° - 89.987°
Number of points	3920
Step size	0.020
Rietveld refinement converged	Yes
Alpha2 subtracted	No
Background subtr.	No
Data smoothed	No
2theta correction	0.02263°
Specimen displacement correction (Bragg-Brentano geometry)	T = (-s/R) = -0.00043661
Radiation	X-rays
Wavelength	1.541874 Å

Analysis Results

Fig. 11. XRD analysis of SnO_2 nanoparticles using MATCH software

For a compound like SnO_2, the weight percentage of each element can be calculated using the molar masses of tin (Sn) and oxygen (O):

Molar Mass of Sn = 118.71 g/mol,
Molar Mass of O = 16.00 g/mol,
Molar Mass of SnO_2 = 118.71 g/mol + 2 × 16.00 g/mol = 150.71g/mol.

The weight fraction of each element is calculated as follows:

$$Weight\ \%\ of\ Sn = \frac{118.71\ g/mol}{150.71\ g/mol}\ x\ 100\%\ \approx 78.8\%$$

$$Weight\ \%\ of\ O = \frac{2\ x\ 16.00\ g/mol}{150.71\ g/mol}\ x\ 100\%\ \approx 21.2\%$$

For the compound SnO_2:

$$Weight\ \%\ of\ Sn = \frac{Molar\ Mass\ of\ Sn}{Molar\ Mass\ of\ SnO_2}\ x\ 100\%$$

$$Weight\ \%\ of\ O = \frac{2\ x\ Molar\ Mass\ of\ O}{Molar\ Mass\ of\ SnO_2}\ x\ 100\%$$

The equations elucidate how the elemental composition percentages are derived from the molar masses of the elements present in the compound.

A. *Characterization of Seaweed*

Fig. 12 shows the sensors response time of approximately 208 seconds when RH fluctuates from 60% to 90%. Initially, the sensor shows a relatively low resistance at 60% RH, indicating minimal water molecule adsorption. As the humidity level rises to 90%, the resistance declines significantly due to the increased adsorption of water molecules on the SnO_2 surface, thereby enhancing conductivity by binding free electrons.

The phenomenon is a characteristic feature of chemo-resistive metal oxide sensors, where the adsorption of water facilitates proton transfer, leading to a reduction in resistance. The sensors show robust responsiveness and sensitivity to changes in humidity, suggesting their potential for applications requiring humidity monitoring.

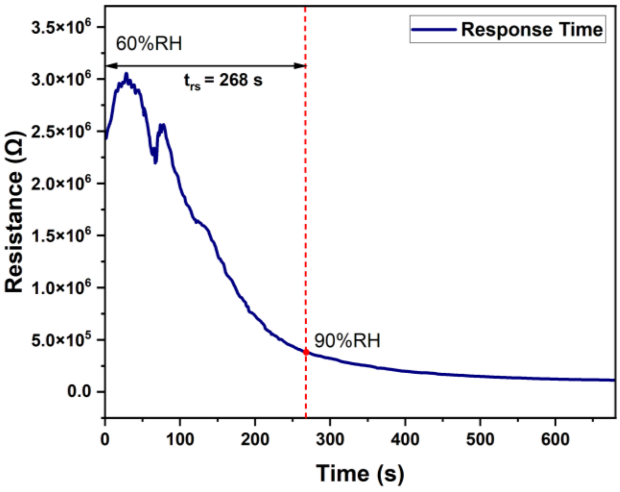

Fig. 12. Response time sensor

Fig. 13 shows the recovery time of sensors in response to a reduction in RH from 90% to 60%. Under elevated humidity, the sensors resistance remains low due to the adsorption of water molecules on its surface, leading to increased conductivity. Following a reduction in humidity (approximately 500 seconds), the resistance increases as water molecules discourage, releasing trapped electrons and reducing conductivity. The recovery time, defined as the interval required for the sensor to attain a stable resistance, is 162 seconds, indicating the sensors rapid response and sensitivity to humidity fluctuations. This behavior is consistent with the typical mechanism of metal oxide sensors, where the adsorption and desorption of water molecules have a significant impact on conductivity.

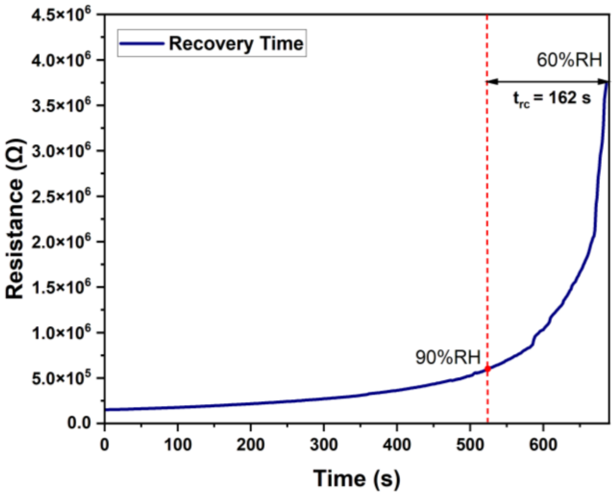

Fig. 13. Recovery time sensor

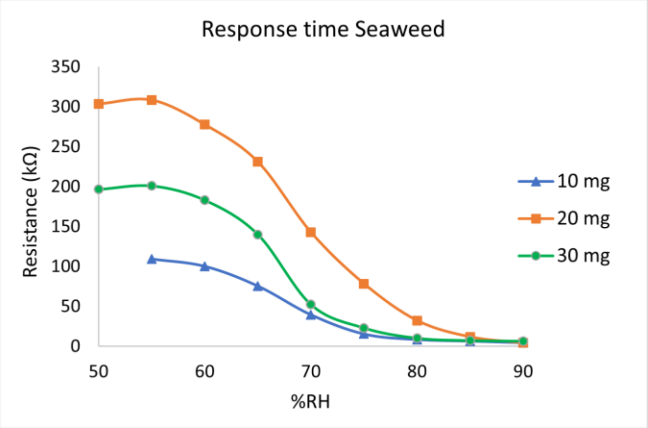

Fig. 14. Response seaweed-based humidity sensor

The relationship between resistance (kΩ) and relative humidity (RH%) for 3 concentrations of the seaweed material (10 mg, 20 mg, 30 mg) during the response is shown in Fig. 14. The 10 mg dose is more sensitive than the 20 mg and 30 mg because the thinner material layer at the lower dose provides a greater surface area open to interacting with water molecules. This increases the number of active sites for adsorption, causing a more rapid alteration in resistance in response to changes in humidity. At 20 mg and 30 mg doses, the thicker coating causes restricted access to active sites and a deceleration in the diffusion of water molecules into the coating, thereby reducing the sensitivity of sensors. Previous studies reported that thinner sensor layers possessed a greater surface area-to-volume ratio, enhancing sensitivity to humidity [30, 31].

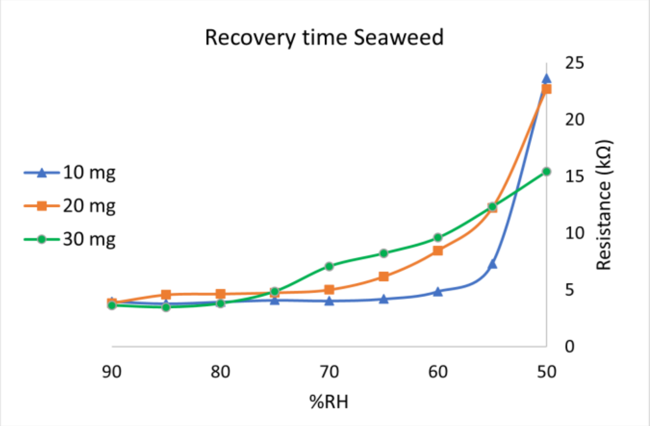

Fig. 15. Recovery seaweed-based humidity sensor

Fig. 15 shows the relationship between resistance (kΩ) and relative humidity (RH%) for 3 concentrations of the seaweed material (10 mg, 20 mg, 30 mg) during the recovery. The 10 mg dose is more sensitive than 20 mg and 30 mg because the thinner material layer has a greater open surface area for interaction with water molecules. At lower doses, the SnO_2 active material accumulates to a lesser extent, thereby increasing the accessibility of the active sites for water adsorption. The direct interaction between water molecules and the sensor surface contributes to variation in resistance regarding humidity monitoring. However, at higher doses, the accumulation of material can reduce the availability of surface sites and impede the diffusion of water molecules, causing a decrease in sensitivity. The results of several studies indicate that a reduction in the coating thickness of semiconductor sensors can enhance sensitivity. This is attributed to an increase in the surface area to volume ratio of the material, which accelerates the interaction with gas or moisture [30, 31]. The exponential equation for response and recovery describes the relationship between changes in sensors resistance over time and the exponential pattern. The following equation illustrates this relationship:

$$R(t) = R_{initial} + \left(R_{final} - R_{initial}\right) x \left(1 - e^{-\frac{t}{\tau}}\right)$$

Where:

$R(t)$ is the resistance at time t.

$R_{initial}$ is the initial resistance.

R_{final} is the final resistance.

τ is the time constant sensor, which indicates how fast the sensor responds or recovers.

To accommodate recovery times, the equation can be modified as follows:

$$R(t) = R_{initial} + \left(R_{final} - R_{initial}\right) x\, e^{-\frac{t}{\tau}}$$

This equation can be solved numerically to find $t_{response}$ and $t_{recovery}$ based on the graph data provided.

To determine the rate of change of resistance concerning humidity (gradient), it is possible to employ the fundamental equation derived from calculus:

$$Slope = \frac{\Delta R}{\Delta RH}$$

Where:

ΔR represents the change in resistance (Ω).

ΔRH denotes the change in relative humidity (%).

The resistance value can be obtained it is necessary to employ the linear interpolation equation:

$$y = y_1 + \frac{(y_2 - y_1)\,.(x - x_1)}{(x_2 - x_1)}$$

Where:

y is the value to interpolate

y_1 and y_2 are known values on the Y-axis

x_1 and x_2 are the known values on the X-axis

x is the X value at the point to interpolate

At the specified coordinates (x_1,y_1) = (70%,180 kΩ) and (x_2,y_2) = (80%,120 kΩ), the resistance value y at 75% RH was interpolated to be 150 kΩ for a sample of 20 mg of seaweed.

V. CONCLUSION

In conclusion, this study explored the synthesis of SnO_2 nanoparticles with high crystallinity and purity through the hydrothermal method. The synthesis process included heating the mixture in an autoclave at 160°C for 12 hours, cooling, filtration, washing with ethanol and deionized water, followed by drying at 100°C for 6 hours. Subsequently, the nanoparticles were subjected to calcination at 500°C for 3 hours to enhance their crystal structure, and ground using an agate mortar for 5 hours. The outcome was SnO_2 nanoparticles with a size of 8.9–9.1 nm.

The resistance of seaweed material was observed to decrease significantly with increasing %RH, particularly at a concentration of 20 mg, which showed the highest resistance of approximately 300 kΩ at low humidity (50% RH). The material showed a high degree of sensitivity to humidity. A concentration of 20 mg showed the highest resistance at low humidity, while 10 mg had a comparatively lower resistance with a more gradual response. The disparate behavior observed at varying concentrations showed that the quantity of seaweed material played an essential in influencing sensors sensitivity and overall performance. The 20 mg sample showed enhanced selectivity and sensitivity, serving as the optimal option for applications in detecting subtle changes in humidity. In comparison, 10 mg sample, with a more gradual response, could be more suitable for environments with less pronounced changes in humidity.

This study examined the response and recovery times of a seaweed-doped SnO_2 thin-film-based humidity sensor with varying doping masses (10 mg, 20 mg, and 30 mg). Based on the response graph, the lower %RH% correlated with longer recovery time, particularly at a doping mass of 30 mg. However, sensors resistance decreased as humidity increased, with higher doping masses causing lower resistance.

ACKNOWLEDGMENT

The authors thank the National Research and Innovation Agency (BRIN) for laboratory access and technical assistance, and Universiti Teknologi Malaysia (UTM) for academic guidance and research collaboration that supported the completion of this research.

REFERENCES

[1] Sajid M, Khattak ZJ, Rahman K, Hassan G, Choi KH. 2022. Progress and future of relative humidity sensors: a review from a materials perspective. *Bull Mater Sci*. 45(4):238. doi:10.1007/s12034-022-02799-x.

[2] Delipinar T, Shafique A, Gohar MS, Yapici MK. 2021. Fabrication and Materials Integration of Flexible Humidity Sensors for Emerging Applications. *ACS Omega*. 6(13):8744–8753. doi:10.1021/acsomega.0c06106.

[3] Ma Z, Fei T, Zhang T. 2023. An overview: Sensors for low humidity detection. *Sensors Actuators B Chem*. 376 PB:133039. doi:10.1016/j.snb.2022.133039.

[4] Juliana N, Mallongi A, Megasari WO. 2021. Analysis Of Humidity, Temperature, Working Period, And Personal Protective Equipment In Home Industry At Gold Craftsmen. *J Ilmu Kesehat*. 9(2):81–89. doi:10.30650/jik.v9i2.2995.

[5] Algün G, Akçay N. 2019. Enhanced sensing characteristics of relative humidity sensors based on Al and F co-doped ZnO nanostructured thin films. *J Mater Sci Mater Electron*. 30(17):16124–16134. doi:10.1007/s10854-019-01982-x.

[6] Toloman D, Popa A, Stan M, Socaci C, Biris AR, Katona G, Tudorache F, Petrila I, Iacomi F. 2017. Reduced graphene oxide decorated with Fe-doped SnO2 nanoparticles for humidity sensor. *Appl Surf Sci*. 402:410–417. doi:10.1016/j.apsusc.2017.01.064.

[7] D. L. Sekulić and T. B. Ivetić, "Characterization of an Impedance-Type Humidity Sensor Based on Porous SnO2/TiO2 Composite Ceramics Modified with Molybdenum and Zinc," Sensors, vol. 23, no. 19, p. 8261, 2023. [Online]. Available: https://www.mdpi.com/1424-8220/23/19/8261.

[8] A. Kumar, P. Kumari, M. S. Kumar, G. Gupta, D. D. Shivagan, and K. Bapna, "SnO_2 nanostructured thin film as humidity sensor and its application in breath monitoring," Ceramics International, vol. 49, no. 15, pp. 24911-24921, Aug 2023, doi: 10.1016/j.ceramint.2023.05.020.

[9] M. Tonezzer, S. C. Izidoro, J. P. A. Moraes, and L. T. T. Dang, "Improved Gas Selectivity Based on Carbon Modified SnO_2 Nanowires," (in English), Frontiers in Materials, Original Research vol. 6, 2019-November-07 2019, doi: 10.3389/fmats.2019.00277.

[10] R. Singh and B. C. Yadav, "Synthesis and Characterization of Copper Doped Tin Oxide for Humidity Sensing Applications," in International Conference on Nanoscience and Nanotechnology, Lucknow, INDIA, Nov 18-20 May-Jun 2013, vol. 20, SI ed., 2014, pp. 895-902, doi: 10.1166/asl.2014.5492.

[11] H. Basavanagoudra et al., "Nanoscopic hygrometry: Exploiting porous nature zinc-doped tin oxide nanoparticles for enhanced humidity sensing at ambient temperature," Sensors and Actuators a-Physical, vol. 370, May 2024, Art no. 115242, doi: 10.1016/j.sna.2024.115242.

[12] W. Zhang et al., "A thin film resistive humidity sensor based on polymer and carbon black nanoparticle composites," Measurement Science and Technology, vol. 35, no. 2, Feb 2024, Art no. 025140, doi: 10.1088/1361-6501/ad0e40.

[13] S. K. Shukla, S. K. Shukla, P. P. Govender, and E. S. Agorku, "A resistive type humidity sensor based on crystalline tin oxide nanoparticles encapsulated in polyaniline matrix," Microchimica Acta, vol. 183, no. 2, pp. 573-580, Feb 2016: 10.1007/s00604-015-1678-2.

[14] S. Q. Wang et al., "Fast response humidity sensor based on chitosan/graphene oxide/tin dioxide composite," Sensors and Actuators B-Chemical, vol. 392, Oct 2023, Art no. 134070, doi: 10.1016/j.snb.2023.134070.

[15] M. V. Arularasu, M. Harb, R. Vignesh, T. V. Rajendran, and R. Sundaram, "PVDF/ZnO hybrid nanocomposite applied as a resistive humidity sensor," Surfaces and Interfaces, vol. 21, Dec 2020, Art no. 100780, doi: 10.1016/j.surfin.2020.100780.

[16] E. Uflyand, V. A. Zhinzhilo, G. D. Kugabaeva, K. K. Kydralieva, and G. I. Dzhardimalieva, "Synthesis of nickel-containing metal-polymer nanocomposites and their use as a humidity sensor," Synthetic Metals, vol. 307, Sep-Oct 2024, Art no. 117709, doi: 10.1016/j.synthmet.2024.117709.

[17] W. Yu, C. Huang, C. Xia, and Z. Q. Wang, "Carbon black nanoparticles modified gelatin composite-based thin film for rapid-response humidity sensing," Measurement Science and Technology, vol. 34, no. 1, Jan 2023, Art no. 015101, doi: 10.1088/1361-6501/ac9801.

[18] X. J. Yun et al., "Fabricating Flexibly Resistive Humidity Sensors with Ultra-high Sensitivity Using Carbonized Lignin and Sodium Alginate," Electroanalysis, vol. 32, no. 10, pp. 2282-2289, Oct 2020, doi: 10.1002/elan.202060128.

[19] J. Zikulnig, S. Lengger, L. Rauter, L. Neumaier, S. Carrara, and J. Kosel, "Sustainable Printed Chitosan-Based Humidity Sensor on

Flexible Biocompatible Polymer Substrate," Ieee Sensors Letters, vol. 6, no. 12, Dec 2022, Art no. 1500804, doi: 10.1109/lsens.2022.3224768.

[20] Kharbanda J, Priya R. 2022. Synthesis and applications of tin oxide nanoparticles: An overview. *Mater Today Proc*. 68:916–921. doi:10.1016/j.matpr.2022.07.131.

[21] Velumani M, Meher SR, Alex ZC. 2018. Impedometric humidity sensing characteristics of SnO2 thin films and SnO_2–ZnO composite thin films grown by magnetron sputtering. *J Mater Sci Mater Electron*. 29(5):3999–4010. doi:10.1007/s10854-017-8342-z.

[22] Neil White, “Thick Films, In book: Springer Handbook of -Electronic and Photonic Materials, pages: 707-721, 2017, DOI: 10.1007/978-3-319-48933-9_29.

[23] Nassar H, Ntagios M, Navaraj WT, Dahiva R. 2018. Multi-Material 3D Printed Bendable Smart Sensing Structures. *Proc IEEE Sensors*. 2018-October October:28–31. doi:10.1109/ICSENS.2018.8589625.

[24] Chen, J., Liu, M., Liu, H., Ma, L., Gao, C., Zhu, S., & Zhang, S. (2010). Synthesis and properties of thermos and pH-sensitive poly (diallyl dimethyl ammonium chloride)/poly (N, N-diethyl acrylamide) semi-IPN hydrogel. *Chemical Engineering Journal*, *159*(1-3), 247-256. https://doi.org/10.1016/j.cej.2010.02.034.

[25] Ilić-Stojanović, S. S., Nikolić, L. B., Nikolić, V. D., Petrović, S. D., Zdravković, A. S. & Stamenković, J. V. (2014). The effect of the cross-linker content on the swelling properties of intelligent gels. *Savremene tehnologije*, *3* (2), 10-15. https://doi.org/10.5937/savteh1402010I.

[26] Povea, M. B., Monal, W. A., Rodriguez, J. V. C., Pat, A. M., Rivero, N. B., & Covas, C. P. (2011). Interpenetrated chitosan-poly (acrylic acid co-acrylamide) hydrogels. Synthesis, characterization, and sustained protein release studies. *Material Sciences and Applications*, *2*, 509-520. http://doi.org/10.4236/msa.2011.26069.

[27] Mahdavinia, G. R., Pourjavadi, A., & Zohuriaan Mehr, M. J. (2006). Convenient one-step preparation of chitosan poly (sodium acrylate co acrylamide) hydrogel hybrids with super swelling properties. *Journal of Applied Polymer Science*, *99*(4), 1615-1619, https://doi.org/10.1002/app.22521.

[28] Desak Gede Sri Andayani, Nuri Astrini, Lik Anah. Optimization of hydrogel CTS-G-PAA/PVA production as adsorbent using response surface methodology (RSM). Leather, Rubber and Plastics Magazine, 34(1), 09-18, 2018. https://doi.org/10.20543/mkkp.v34i1.3435.

[29] Li W, Liu J, Ding C, Bai G, Xu J, Ren Q, Li J. 2017. Fabrication of Ordered SnO2 Nanostructures with Enhanced Humidity Sensing Performance. *Sensors*. 17(10):2392. doi:10.3390/s17102392.

[30] Su, P.-G.; Hsu, H.-C.; Liu, C.-Y. Layer-by-Layer Anchoring of Copolymer of Methyl Methacrylate and [3-(methacrylamino)propyl] Trimethyl Ammonium Chloride to Gold Surface on Flexible Substrate for Sensing Humidity. *Sens. Actuators B Chem.* **2013**, *178*, 289–295.

[31] E. Comini, C. Baratto, G. Faglia, M. Ferroni, A. Vomiero, G. Sberveglieri, “Quasi-one dimensional metal oxide semiconductors: Preparation, characterization and application as chemical sensors”, Progress in Materials Science, Volume 54, Issue 1, January 2009, Pages 1-67.